



First-Principles study of the structural, electronic, elastic, lattice dynamics and thermoelectric properties of the newly predicted half-heusler alloys NaYZ (Z = Si, Ge, Sn)

Olusola G. Adeleye ^{a,*}, Bamidele I. Adetunji ^{b,**}, Abdulahi N. Njah ^a, Olasunkanmi I. Olusola ^a

^a University of Lagos, Faculty of Science, Physics Department, Yaba, Lagos State, Nigeria
^b Bells University of Technology, Physical Sciences Department, Ota, Ogun State, Nigeria



ARTICLE INFO

Communicated by: Luis Brey

ABSTRACT

In this study, we applied Density Functional Theory (DFT) and Boltzmann Transport Theory to investigate the structural, electronic, lattice dynamic, elastic and thermometric properties of new half-Heusler compounds NaYZ (Z = Si, Ge, Sn). The structural optimization calculations revealed that the ZXY (1/4, 1/2, 0) phase have the most stable state with the least energy among others. Our calculated lattice constants in (Å) are found to be 6.861, 6.899, and 7.284 for NaYZ (Z = Si, Ge, Sn). Also, the calculated elastic constants satisfied the Born-Huang criteria and were found to be mechanically and elastically stable. The Density Functional Perturbation Theory (DFPT) was used to examined the lattice dynamics of the compounds and the results shown non-existence of negative frequencies all through dispersion band structures, thus all the compounds are dynamically stable. The Seebeck coefficient of the compounds at room temperature for the p-type (n-type) are 143.79 (-48.91) μ V/K, 132.49 (-48.86) μ V/K, 154.75 (-60.24) μ V/k for NaYZ (Z = Si, Ge, Sn). The modified Slack's approach was used to compute lattice thermal conductivity (k_p) within the experimental range and the k_p values obtained for NaYZ (Z = Si, Ge, Sn) at room temperature are 17.265 W m⁻¹ K⁻¹, 14.671 W m⁻¹ K⁻¹, 10.693 W m⁻¹ K⁻¹, respectively. The computations of charge carriers relaxation time ($\tau = F(T)$) as a function of temperature through deformation potential theory and the effective mass of charge carriers were used to evaluate the figure of merit (zT) for p-type and n-type of the materials. The maximum zT at 1200 K of $\tau = F(T)$ ($\tau = 10^{-13}$ s) are 1.76 (1.67), 1.73 (1.65), and 1.91 (1.88). These results show that $\tau = F(T)$ has improvement in determining the figure of merit as compared to the constant relaxation time (τ).

1. Introduction

The quest for clean and reliable power source has led to an increase in the demand for energy materials that can effectively convert heat to electricity. Over the past few decades, a range of materials for the conversion of heat to electricity have been discovered as a result of this demand [1-3]. This waste heat conversion to energy relies on a thermoelectric (TE) mechanism that employs environmentally friendly thermoelectric materials. Thermoelectric efficiency which is directly proportional to how much energy can be recovered from heat is the sole determining factor for thermoelectric systems. The dimensionless parameter known as the figure-of-merit (zT) is used to compute the

efficiency of thermoelectric device. The Seebeck coefficient S, electrical conductivity σ , power factor $S^2\sigma$ and κ , the total of the thermal contributions from the electron (k_e) and phonon (k_p) all have direct impact on zT according to $zT = \frac{S^2\sigma T}{\kappa}$. A high power factor and low thermal conductivity can be used to obtain a significant value of the zT parameter. Therefore, Increasing the power factor and lowering the lattice thermal conductivity of TE using some approaches such as doping, band engineering, and material dimension reduction [4,5] will promote the efficiency of TE materials.

Among the notable categories of energy materials, Heusler alloys and half-Heusler alloys are known to exhibit a variety of applications in photovoltaic devices, solar cell devices, catalysis, fuel cell, and ther-

* Corresponding author.

** Corresponding author.

E-mail addresses: researchwqe@gmail.com (O.G. Adeleye), biadetunji@bellsuniversity.edu.ng (B.I. Adetunji), anjah@unilag.edu.ng (A.N. Njah), iolusola@unilag.edu.ng (O.I. Olusola).

moelectric devices [6–9]. Half-Heusler materials are good candidates for thermoelectric applications due to their high power factors, narrow band-gaps, and mechanical stability [10–13]. Half-Heusler alloys are composed of three elements XYZ with space group of F43 m and crystallized in C1_b structure, where X and Y are earth elements or transition elements and Z element as main group in the periodic table [14].

In order to determine the thermoelectric efficiency zT of half-Heusler materials, either constant relaxation time (τ) or relaxation time temperature-dependent ($\tau = F(T)$) calculations can be used [15,16]. The semi-classical Boltzmann transport theory is frequently used to compute the transport parameters of materials under the constant relaxation time assumption [17]. Under the constant relaxation time assumption, only σ and k_e in exception to Seebeck coefficient S, are closely related to τ . In addition, the electronic figure-of-merit $zT_e = \frac{S^2 \sigma T}{k_e}$ only has an inverse relationship with k_e and a direct relationship with σ [17]. However, because the phonon contribution (k_p), which is a component of the denominator and is independent of τ , τ computation is required for correct assessment and analysis of thermoelectric efficiency [18].

Numerous studies have been conducted on half-Heusler alloys in the recent years, including those based on Lithium, Rhodium, and Potassium compounds [19–21]. For instance, in the study of Kamlesh et al. [22], the electronic, optoelectronic, and thermoelectric properties of XScZ (X = Li, Na, K; Z = C, Si, Ge) were examined using a full potential linearized plane wave with density functional theory and Boltzmann theory within a constant relaxation time approximation. The half-Heusler alloys were found to have direct band gaps ranging from 0.94 eV to 1.64 eV, indicating that they are semiconductors. Due to their almost unity values of zT at room temperature, all the compounds were considered to be effective thermoelectric materials. Utilizing full-potential linearized augmented plane wave (FP-LAPW) and the BoltzTraP code, Cherchab et al. [23] investigated the structural stability and thermoelectric characteristics of HH KLaX (X = C, Si, Ge, and Sn) compounds. The authors reported that the thermopower and Seebeck coefficient values for these half-Heusler alloys were significantly high. Also, the thermoelectric capabilities of PCdNa were examined by Xianfeng Ye et al. [24], and found that the material has a figure-of-merit (zT) of 3.3 at 900 K for ideal p-type doping. Furthermore, Anuradha et al. investigated how temperature relaxation time influences the thermoelectric characteristics of LiScX (X = C, Si, and Ge) materials. According to their investigation, they found out that figure-of-merit obtained with temperature dependent relaxation time which were 0.476, 0.573 and 0.671 were better than that of constant relaxation time of 10fs which were 0.40, 0.15, and 0.11 for LiScX (X = C, Si, and Ge). Therefore, the use of temperature dependent relaxation time had been found to have substantial effect along with improved figure-of-merit in comparison to the constant relaxation time.

Motivated by the literature outlines above, the current work aims at investigating the structural properties, electronic properties, lattice dynamics, elastic properties, transport properties, lattice thermal conductivity and temperature dependent relaxation time effects on figure-of-merit of the compounds NaYZ (Z = Si, Ge, Sn). Therefore, to the best of our knowledge it is interesting to know that there are no previous studies on NaYZ (Z = Si, Ge, Sn).

2. Computational methods

In this work, the structural, electronic, lattice dynamics and elastic properties of the half-Heusler alloys NaYZ (Z = Si, Ge, Sn) were investigated with DFT and pseudopotential plane wave methods as implemented in Quantum espresso code [25]. The projected augmented-wave (PAW) pseudopotentials sourced from pslibrary [26] were used to describe the exchange-correlation effect. The cutoff energy and k-points mesh for wave function and Brillouin zone integrations are 90 Ry and 12 x 12 x 12 respectively. The Density Functional Perturbation theory (DFPT) [27] was used to compute the lattice dynamics of the

compounds. The stress-strain method as implemented in thermo_pw code were used to determine the elastic constants within the range of -0.0075 to +0.0075 at a step of 0.005 [28,29].

The transport properties of NaYZ compounds were examined with semi-classical Boltzmann transport theory as implemented in BoltzTrap2 code [30]. We employed deformation potential theory proposed by Bardeen and Shockley [31,32] to compute temperature dependent relaxation time as stated by equation (1). The deformation potential (E_a) is defined as change in the valence band edge or conduction band edge of the band structure corresponding to fractional change in the lattice constants along x-axis (see equation (2)). The effective masses of the charge carriers, electron (m_e^*) and hole (m_h^*) were computed using a direct expression of $m^* = \frac{\hbar^2}{\left(\frac{d^2E}{dx^2}\right)^{-1}}$ with the minimum conduction band curvature and the maximum valence band curvatures respectively.

$$\tau = \frac{2\sqrt{2\pi}\hbar^4 C_{11}}{3E_a^2(m^*k_B T)^{\frac{3}{2}}} \quad (1)$$

And

$$E_a = \frac{\delta E_{edge}}{\delta \left(\frac{\Delta a}{a_0} \right)} \quad (2)$$

where C_{11} , m^* , E_a , and T are elastic constant along x-axis, effective mass of charge carrier, deformation potential, and temperature in Kelvin respectively. Lattice thermal conductivity k_p of the half-Heusler compounds were calculated using an optimized slack model as to fashion our results within the experimental range as referenced in Ref. [33]. This optimized Slack model is expressed with equations (3) and (4) below. Equation (3) comprises \overline{M}_a , δ , n and θ which are average atomic mass in amu, volume per atom in \AA^3 , number of atoms present in the primitive cell, and acoustic Debye temperature (Θ_a) measured in Kelvin. Equation (4) is an expression of Gruenes parameter (γ) that depends completely on Poisson ratio ($\gamma = \frac{3}{2} \frac{1+v}{2-3v}$), where v is the Poisson ratio.

$$k_p = A_{optimized} \frac{\overline{M}_a \delta n^{1/3} \Theta_a^3}{\gamma^2 T} \quad (3)$$

and

$$A_{optimized} = \frac{1}{1 + \frac{1}{\gamma} + \frac{8.3 \times 10^5}{\gamma^{2.4}}} \quad (4)$$

3. Results and discussion

3.1. Structural optimization and electronic properties

The half-Heusler compounds of NaYZ (Z = Si, Ge, Sn) crystallized in their identical form as the face-center-cubic structure of MgAgAs-type with the space group F-34 m. The atomic positions of NaYZ (0, 1/2, 1/4), YZNa (1/4, 0, 1/2), and ZNaY (1/4, 1/2, 0) are applied to determine the ground-state structural arrangement.

The graphs of total energy against unit-cell volume in phases XYZ, YXZ, and ZXY are used to represent the ground state calculations in Fig. 1. We observe from these graphs that the lowest energy configuration corresponds to the material with the most stable phase and ground-state atomic positions.

By fitting the curve of total energy against unit-cell volume into Birch-Murnaghan's equation of state [34], the optimized structural properties, including lattice constant, bulk modulus (B), pressure derivative of bulk modulus (B'), minimum energy E_0 , and minimum volume (V_0), were obtained. The results of this procedure are shown in Table 1 with different atomic configurations, minimum energies, lattice constants, bulk moduli, and minimum volumes. As can be seen by comparing the minimum energies for each distinct atomic configuration,

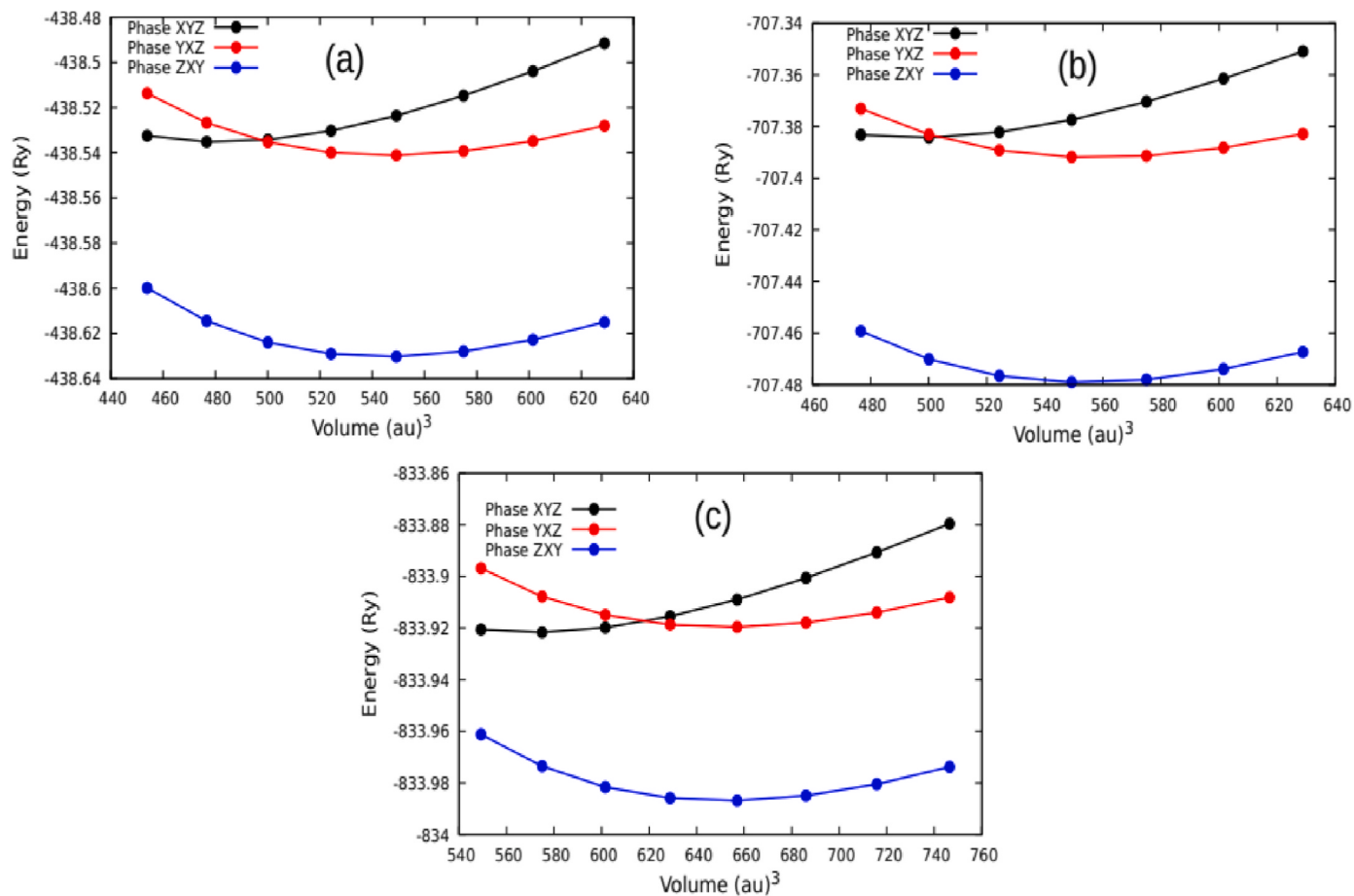


Fig. 1. Structural optimization of NaYZ (Z = Si, Ge, Sn) (a) NaYSi, (b) NaYGe, (c) NaYSn as a function of energy against unit cell volume.

Table 1

The Calculated Ground state Configuration with Different Phases of Energy(E_0), Lattice Constants in Å, Bulk Modulus (B) in GPa and Derivative of Bulk Modulus (B') for NaYZ (Z = Si, Ge and Sn).

Half-Heusler	E_0 (Ry)	(a(Å))	B(GPa)	B'	$V_0(\text{Å}^3)$
XYZ (1/4, 1/2, 0)					
NaYSi	-438.53537	6.584	46.90	4.88	71.38
NaYGe	-707.38435	6.647	43.10	5.01	73.43
NaYSn	-833.92176	6.863	39.10	5.12	80.81
YXZ (1/4, 0, 1/2)					
NaYSi	-438.54116	6.866	38.20	3.81	80.93
NaYGe	-707.39194	6.915	36.00	3.98	82.67
NaYSn	-833.91961	7.178	31.30	3.93	92.47
ZXY (1/4, 1/2, 0)					
NaYSi	-438.63033	6.861	43.70	3.78	80.76
NaYGe	-707.47903	6.899	41.80	3.98	82.09
NaYSn	-833.98688	7.284	35.10	3.79	96.62

the ZXY phase has the lowest minimum energy and is also the most stable atomic configuration, as was previously proven by comparing the energy against unit-cell volume in Fig. 1. As a result, we choose the ZXY phase arrangement since those atomic positions are the most stable.

Table 2

The Optimized Lattice Constants(a(Å)), Calculated Band gaps (PBE), Effective Masses of Electron and Hole, Deformation Potential of Electron($E_{\alpha(e)}$), Deformation Potential of hole($E_{\alpha(h)}$), Relaxation time of Charge Carriers (τ_e, τ_h) at room Temperature for the half-Heusler alloys NaYZ (Z = Si, Ge, and Sn).

Compounds	(a(Å))	Band-gap (eV)	m_e	m_h	$E_{\alpha(e)}$ (eV)	$E_{\alpha(h)}$ (eV)	τ_e (fs)	τ_h (fs)
NaYSi	6.861	0.535	0.270	0.290	2.0126	2.0014	5640.70	4720.60
NaYGe	6.899	0.571	0.269	0.271	1.4875	1.7367	9206.36	6697.20
NaYSn	7.284	0.653	0.490	0.830	1.4971	1.4849	2807.60	1294.50

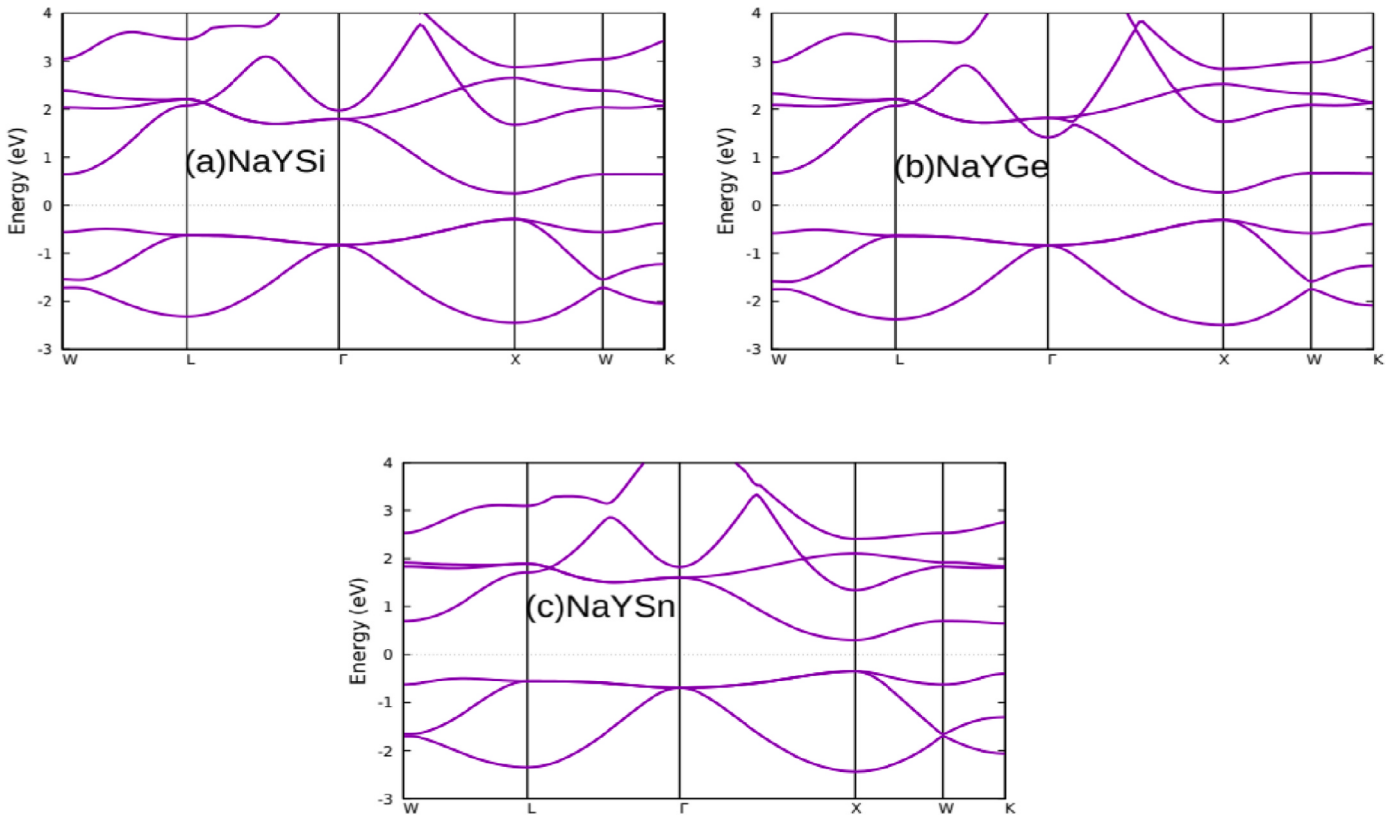


Fig. 2. The calculated band structures of NaYZ ($Z = \text{Si, Ge, and Sn}$) (a)NaYSi, (b) NaYGe, (c) NaYSn.

charge carriers hole (m_h) and electron (m_e) were determined using a straightforward expression of $m^* = \frac{\hbar^2}{\left(\frac{d^2E}{dk^2}\right)^{-1}}$ with the minima conduction band and maxima valence band curvatures, respectively. The results of the effective masses of electron and hole are shown in Table 2 and they suggest that the compounds would have better thermoelectric performance in the p-type region than the n-type region because the Seebeck coefficients are always increased by the effective masses of charge carriers [37].

The calculated partial density of states (PDOS) and total density of states (TDOS) results are presented in Figs. 3 and 4 respectively. The PDOS of all the compounds have the valence band portion ranges from -3 eV to 0 eV while conduction band extends from 0 eV to 4 eV . The PDOS of the conduction region for NaYZ compounds has a single significant contribution of Y(d) orbital at around 2 eV energy for all the compounds, and a small orbitals mixing of Na (p), Z (p), Y (p) and Y (s) from 0 eV to 4 eV . The orbitals of Y (d) and Ge (p) have contributions close to Fermi level in NaYGe and NaYSn compounds conduction band regions while for NaYSi compound only Y (d) orbital contribution is seen as shown in the Fig. 3 (a). The valence region of PDOS are dominated by Z (p) and Y (d) orbitals with higher contribution from Z (p) orbital. A hybridized dense states is observed closer to the Fermi level, common to all the compounds in the valence region. This dense state consists of contributions from Na (p), Y (p), Z (p) and Y (d) orbitals, an attribute of p-type semiconductor materials favourable for thermoelectric properties in this region [38]. The calculated total density of states (TDOS) of NaYZ ($Z = \text{Si, Ge, Sn}$) results show that the valence region has higher energy state contributions compared to the conduction band region. The highest peak of the TDOS corresponds to flat band edge (heavy m_h). It is obvious from the TDOS of the valence regions that Fig. 4 (c) has the highest peaks compared to others. This suggests a flatten band edge with massive charge carriers (m_h and m_e) as previously predicted, calculated and shown in Table 2.

4. Lattice dynamics

The phonon dispersion bands of half-Heusler NaYZ ($Z = \text{Si, Ge, Sn}$) compounds plotted along Γ -X- Γ -L-X-W-L symmetry points are presented in Fig. 5. Each phonon band has three acoustic modes and six optical modes created by the three atoms that make up the NaYZ ($Z = \text{Si, Ge, Sn}$) primitive unit cell. The maximum acoustic frequencies are 133.20 cm^{-1} , 128.94 cm^{-1} , 105.06 cm^{-1} for NaYZ ($Z = \text{Si, Ge, Sn}$), respectively; a consistent range of acoustic frequency peculiar to half-Heusler alloys [39] and this reduction in acoustic frequencies indicate a decline in the related group velocity, which would further reduced lattice thermal conductivity in this same order [40]. Additionally, the observed drop in acoustic mode frequencies from NaYSi to NaYSn compounds could be attributed to an increase in atomic radius and atomic mass number in NaYZ ($Z = \text{Si, Ge, Sn}$) as both grow down the group on the periodic table. As the mass of the element (Z) increases, it is therefore anticipated that the frequency of phonon vibrations will decrease. In all the phonon dispersion bands, the acoustic and optical modes have energy phonon gaps (phonon-phonon scattering). Since a smaller or narrower phonon gap is beneficial to low lattice thermal conductivity (k_p), k_p decreases as the atomic mass of Z (Si, Ge, Sn) increases. The NaYSn compound would have the lowest k_p compared to the other compounds, following the same trend as acoustic frequencies. Also, low k_p is one of the main features of good thermoelectric materials [41], and the thermoelectric performance of the compounds would be in the order of NaYSn, NaYGe, and NaYSi, respectively. The absence of imaginary frequencies in the broad dispersion band range for all the compounds serves as confirmation of their dynamics and stability.

5. Mechanical properties

Understanding a material's elastic constants is crucial for analyzing its mechanical stability, strength, hardness, ductility, and stiffness. The

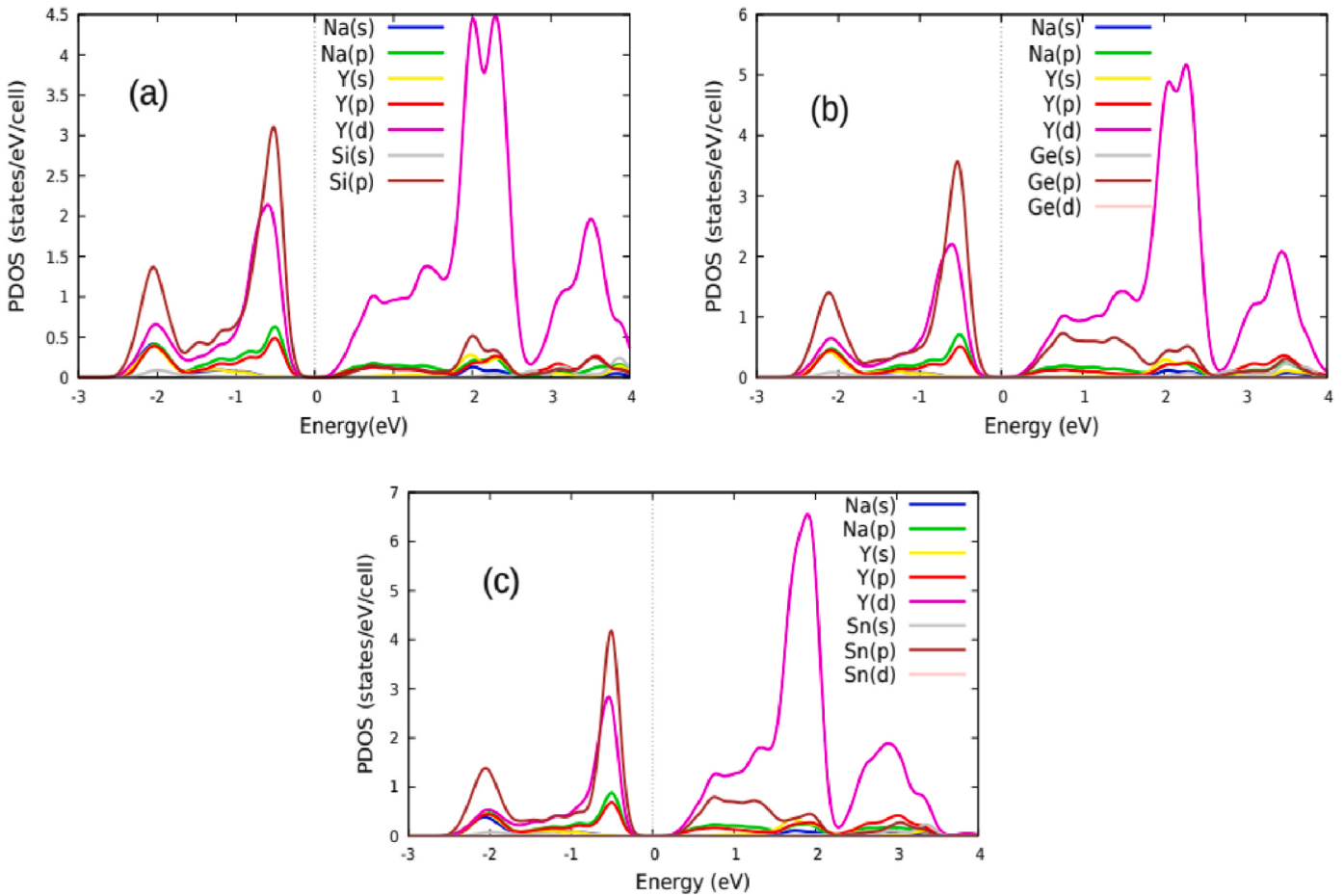


Fig. 3. The calculated partial density of state (PDOS) of NaYZ ($Z = \text{Si, Ge, and Sn}$) (a) NaYSi, (b) NaYGe, (c) NaYSn compounds.

computed cubic elastic constants C_{11} , C_{12} and C_{44} of half-Heusler NaYZ ($Z = \text{Si, Ge, Sn}$) along with other mechanical parameters are presented in Table 3.

The elastic constants of these half-Heusler alloys are subjected to Born-Huang criteria ($C_{11}-C_{12} > 0$, $C_{44} > 0$, $C_{11} + 2C_{12} > 0$, $C_{11} > 0$, and $C_{12} < B < C_{11}$) [42] to validate the materials mechanical stability. These criteria are fully satisfied and we conclude that NaYZ ($Z = \text{Si, Ge, Sn}$) compounds are elastically and mechanically stable. The elastic constants C_{11} of NaYSi compound is greater than others. This shows NaYSi compound has greater resistance against strain compared to others. Similarly, the value of C_{44} for NaYSi is greater than NayGe and NaySn; which means NaYSi has higher tendency against shear deformation compared with others. The stiffness of a material and bond strength is measured by Young modulus (E) [43], and E reduces with increase in atomic number from Si to Sn element as shown with the calculated values in Table 3. This reveals that NaYSi compound is stiffer and have the highest bond strength among others. The bulk modulus of the compounds NaYZ ($Z = \text{Si, Ge, Sn}$) computed in ground state calculations for structural optimizations as shown in Table 2 are in good agreement with thermo_pw results shown in Table 3. A material can either exhibits a directional oriented property or non-directional. This property is determined by Shear anisotropy (A), expression given as

$$A = \frac{2C_{44}}{C_{11} - C_{12}} \quad (5)$$

If A is less than one or larger than one, a material has anisotropic properties; if A is equal to one, it has isotropic properties. The calculated values of A are 0.79, 0.81, and 1.05 for NaYZ ($Z = \text{Si, Ge, Sn}$), respectively. These values confirmed that all the compounds are anisotropic (A) in nature. The brittle or ductile nature of materials is determined by the

ratio of bulk modulus (B) to shear modulus known as Pugh's ratio. The critical Pugh's ratio value is 1.75. A material is brittle in nature if B/G is less than 1.75 and ductile if B/G exceeds 1.75. Our calculated B/G values as shown in Table 3 are all less than 1.75; thus all the compounds are brittle in nature. The ratio of bulk modulus (B) to shear modulus (G) is (Frantsevich's ratio) known to determine the extent of resistance of a material against shear deformation. The standard limit (1.06) of Frantsevich's ratio is greater than all the calculated B/G ratios, this confirmed that all the half-Heusler NaYZ ($Z = \text{Si, Ge, Sn}$) alloys have low resistance to shear deformation. The bonding type of crystals are determined with Poisson ratio (ν). The bonding type is covalent if ν is 0.1 and ionic for 0.25. The calculated values of ν show that NaYSi and NaySn compounds have ionic bonding while NayGe compound possesses covalent bonding [44]. The Cauchy pressure C is an expression of the difference between C_{12} and C_{44} elastic constants. Its negative and positive values tentatively define a material's nature being brittle (covalent) or ductile (ionic) respectively. It is obvious from the Table 3 that NaySi and NayGe compounds are brittle in nature with negative Cauchy pressure values, while NaySn is ductile with positive Cauchy pressure C . A key thermodynamic parameter that relates closely with elastic constants is known as the Debye temperature (θ_D). It is intimately connected and used to measure numerous physical properties including melting point, thermal expansion, and specific heat [45]. Additionally, Debye temperature explains the robustness of solid-state bonding and structural stability [46]; it also reflects bond strength of materials, as high θ_D signifies strong atomic bonding while low θ_D denotes weak atomic bonding [47]. In Table 3, the θ_D computed decreases as Z moves from Si to Sn element. This trend is also predicted for lattice thermal conductivity k_p under lattice dynamics, and confirmed due to θ_D direct relation

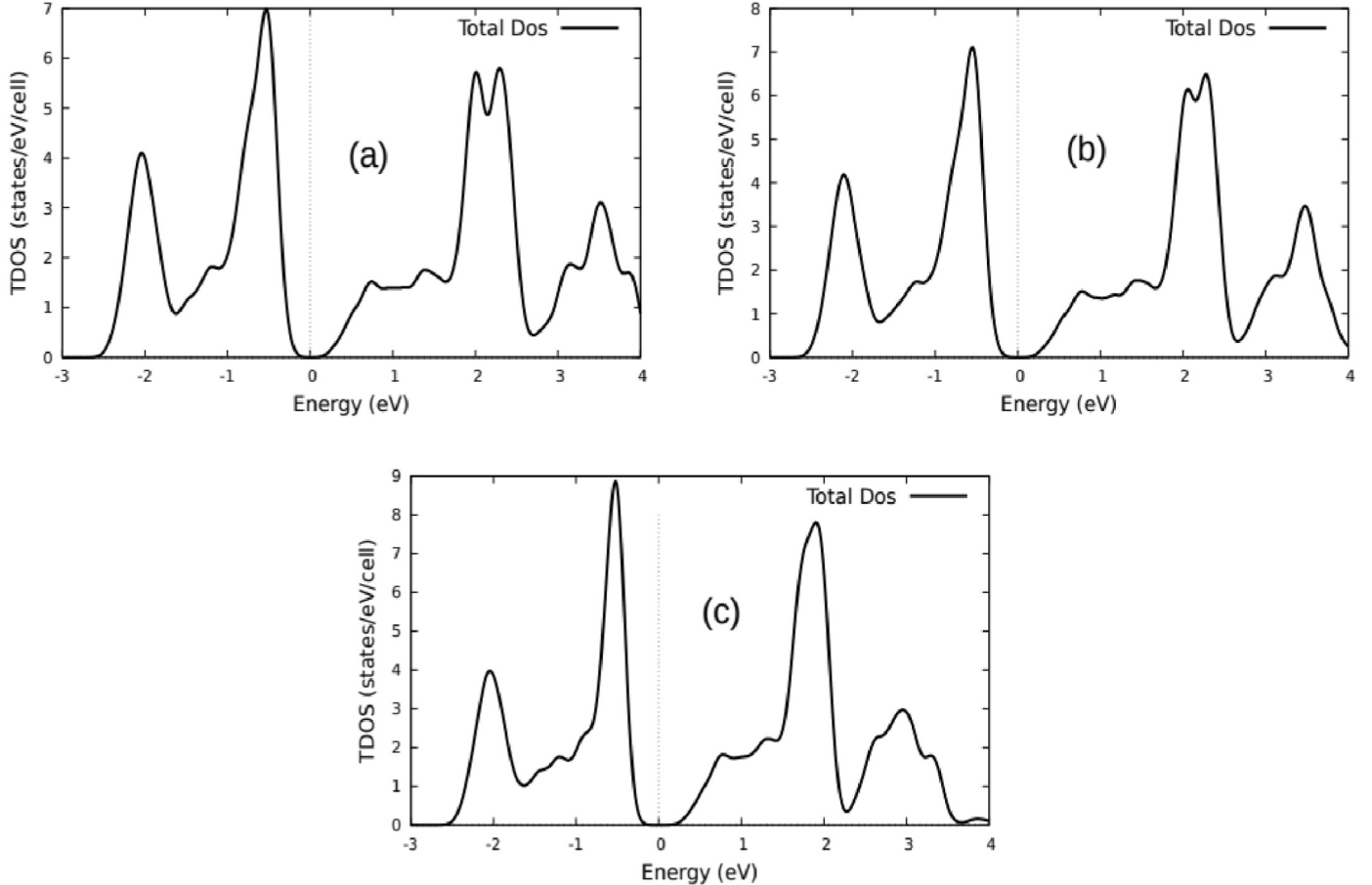


Fig. 4. The calculated total density of State (DOS) of NaYZ (Z = Si, Ge, and Sn) (a) NaYSi, (b) NaYGe, (c) NaYSn compounds.

with k_p as expressed by Equation (3). Debye temperature (θ_D) can be evaluated from the elastic constants with average sound velocity (v_m) as illustrated by the following formula.

$$\theta_D = \frac{h}{k_B} \left(\frac{3n}{4\pi} \frac{N_A \rho}{M} \right)^{\frac{1}{3}} v_m \quad (6)$$

where n , N_A , h , k_B are number of atoms in the primitive cell, Avogadro's Constant, Planck Constant, and Boltzmann Constant, respectively. The average sound velocity v_m is given as

$$v_m = \left[\frac{1}{3} \left(\frac{2}{v_t^3} + \frac{1}{v_l^3} \right) \right]^{\frac{1}{3}} \quad (7)$$

v_t , v_l are the transverse and longitudinal sound velocities respectively. Both v_t and v_l are defined as stated by the following equations

$$v_t = \left(\frac{G}{\rho} \right)^{\frac{1}{2}} \quad (8)$$

and

$$v_l = \left(\frac{B + \frac{4}{3}G}{\rho} \right)^{\frac{1}{2}} \quad (9)$$

where G is the shear modulus, B is the bulk modulus and ρ density of the solid. Sound velocities through materials are closely related to the bond strength of the material scaled with Young modulus as illustrated [48] by the equation

$$E = \frac{\rho v_t^2 (3v_l^2 - 4v_t^2)}{v_l^2 - v_t^2} \quad (10)$$

This suggests that high bond strength of the materials is associated with high sound velocities. And from the calculated values in Table 3, both E and v_m decrease as Z atomic mass increases from Si to Sn. The weaker the bond strength the smaller the E and v_m , both tend to follow same trend. The bond strength of the half-Heusler compounds under consideration increase in this order NaYZ (Z = Sn, Ge, Si).

6. Thermoelectric properties

The thermoelectric properties such as Seebeck coefficient (S), electrical conductivity (σ), thermal conductivity (k) and the figure of merit of half-Heusler compounds NaYZ (Z = Si, Ge, Sn) were computed via rigid band approximation in Boltzmann transport equation as implemented in BoltztraP2 code.

6.1. Seebeck coefficient

Fig. 6 displays the Seebeck coefficients of the compounds NaYZ (Z = Si, Ge, Sn) as a function of temperature for both p and n type charge carriers. The rise in temperature sharply increases the Seebeck coefficient (S) for the p-type charge carrier but the pattern for the n-type is the opposite. The S in the p-type region of NaYZ (Z = Si, Ge, and Sn) are $143.79 \mu \text{V/K}$, $132.49 \mu \text{V/K}$, $154.75 \mu \text{V/K}$, respectively, at room temperature. The overlapping of the curves in **Fig. 7(b)** is due to the fact that the S value for NaYSn on the n-type region is $-60.24 \mu \text{V/K}$, whereas the values of S for NaYSi and NaYGe are roughly equivalent ($-48.91 \mu \text{V/K}$ and $-48.86 \mu \text{V/K}$, respectively). According to Mott's formula,

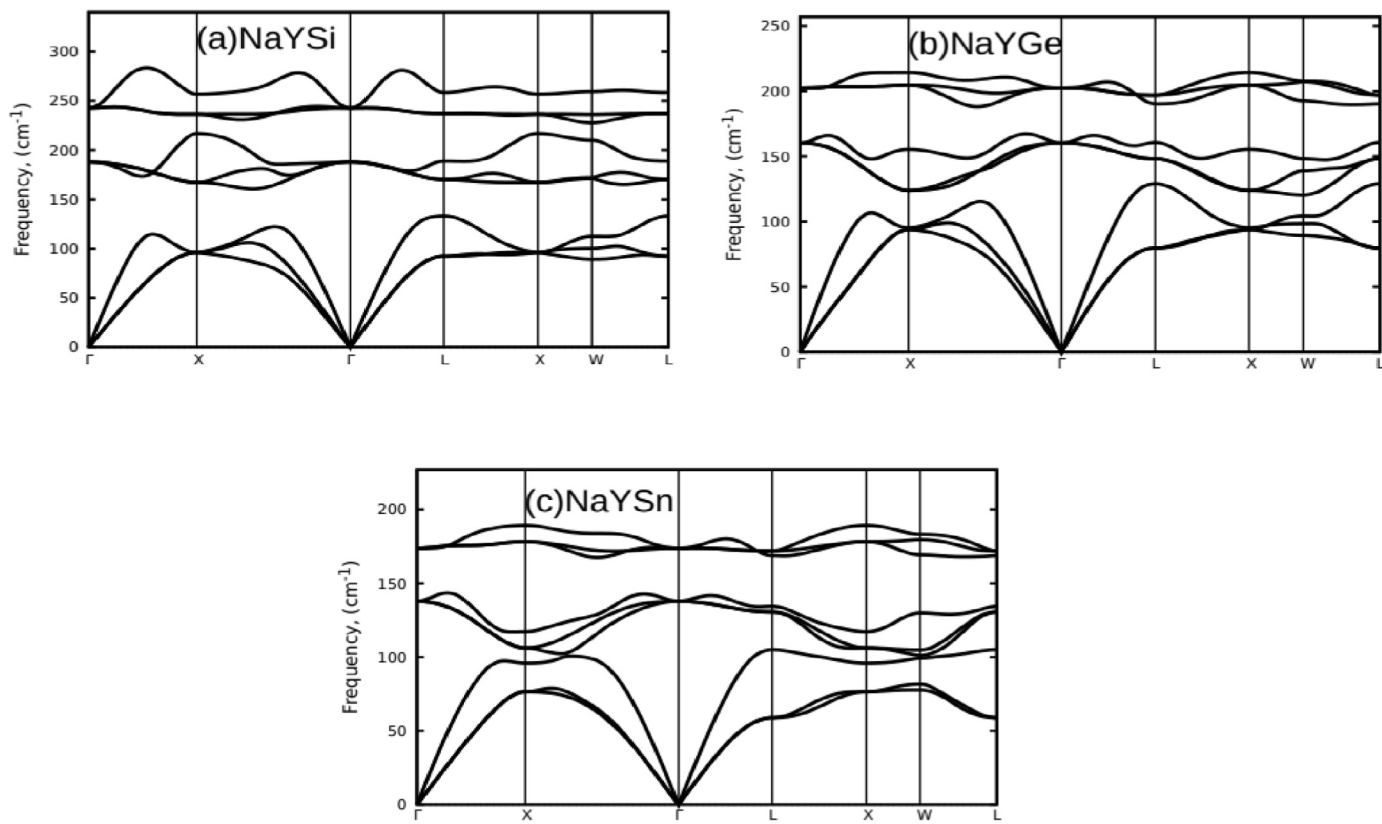


Fig. 5. Phonon dispersion bands of NaYZ ($Z = \text{Si}, \text{Ge}, \text{Sn}$) (a) NaYSi, (c) NaYGe, and (c) NaYSn of half-Heusler compounds.

Table 3

The elastic constants (C_{11}, C_{12}, C_{44}), Young Modulus (E), Shear Modulus (G), Bulk Modulus (B), Pugh's Ratio (B/G), Frantsevichs ratio(G/B) Poisson Ratio (v), Cauchy Pressure ($C_{12}-C_{44}$), Grunesen Parameter (γ), Debye Temperature (Θ_D), Density ($\rho/\text{kg/m}^3$), Transverse Sound Velocity(v_t), Longitudinal Sound Velocity(v_l), Average Sound Velocity (v_m) for the half-Heusler alloys of NaYZ ($Z = \text{Si}, \text{Ge}, \text{Sn}$).

Crystal	C_{11}	C_{12}	C_{44}	E(GPa)	G(GPa)	B(GPa)	B/G	G/B	v	$C_{12}-C_{44}$	γ	$\Theta_D(\text{K})$	$\rho(\text{kg/m}^3)$	$v_t(\text{m/s})$	$v_l(\text{m/s})$	$v_m(\text{m/s})$
NaYSi	84.87	23.78	24.32	66.39	26.64	44.14	1.66	0.60	0.25	-0.54	1.49	335.49	2879.10	3041.97	5260.16	3376.67
NaYGe	81.68	22.41	24.02	64.96	26.13	42.17	1.61	0.62	0.24	-1.61	1.47	289.97	3732.96	2645.46	4541.65	2934.65
NaYSn	61.87	21.93	20.92	51.58	20.53	35.24	1.72	0.58	0.26	1.01	1.53	236.62	3964.99	2275.59	3973.96	2528.14

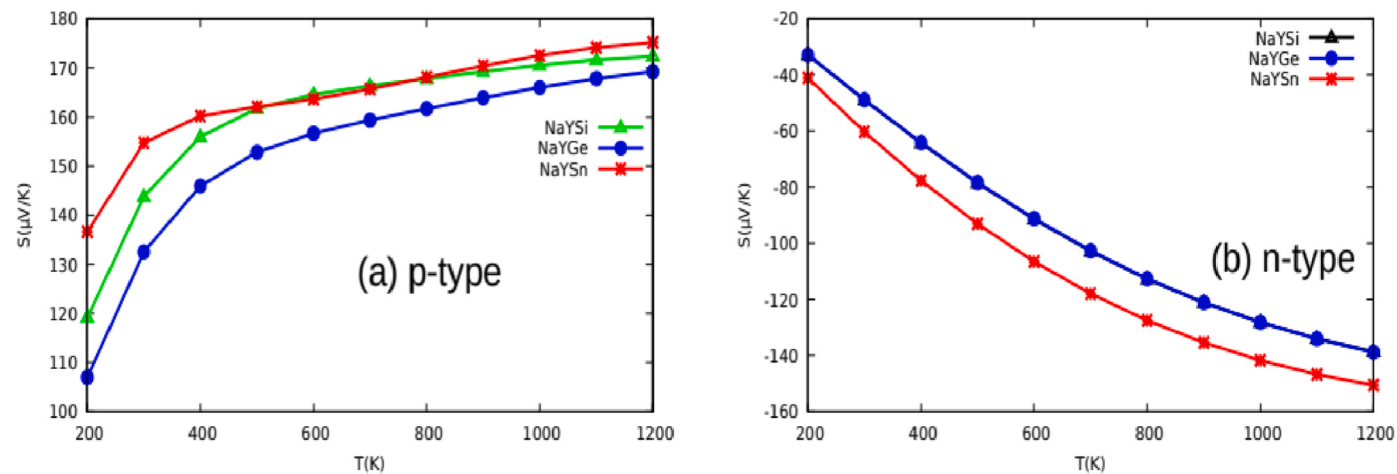


Fig. 6. The Seebeck coefficient as a function of temperature (200 K-1200 K) for both (a) p-type and (b) n-type carriers of NaYZ ($Z = \text{Si}, \text{Ge}, \text{Sn}$) half-heusler compounds.

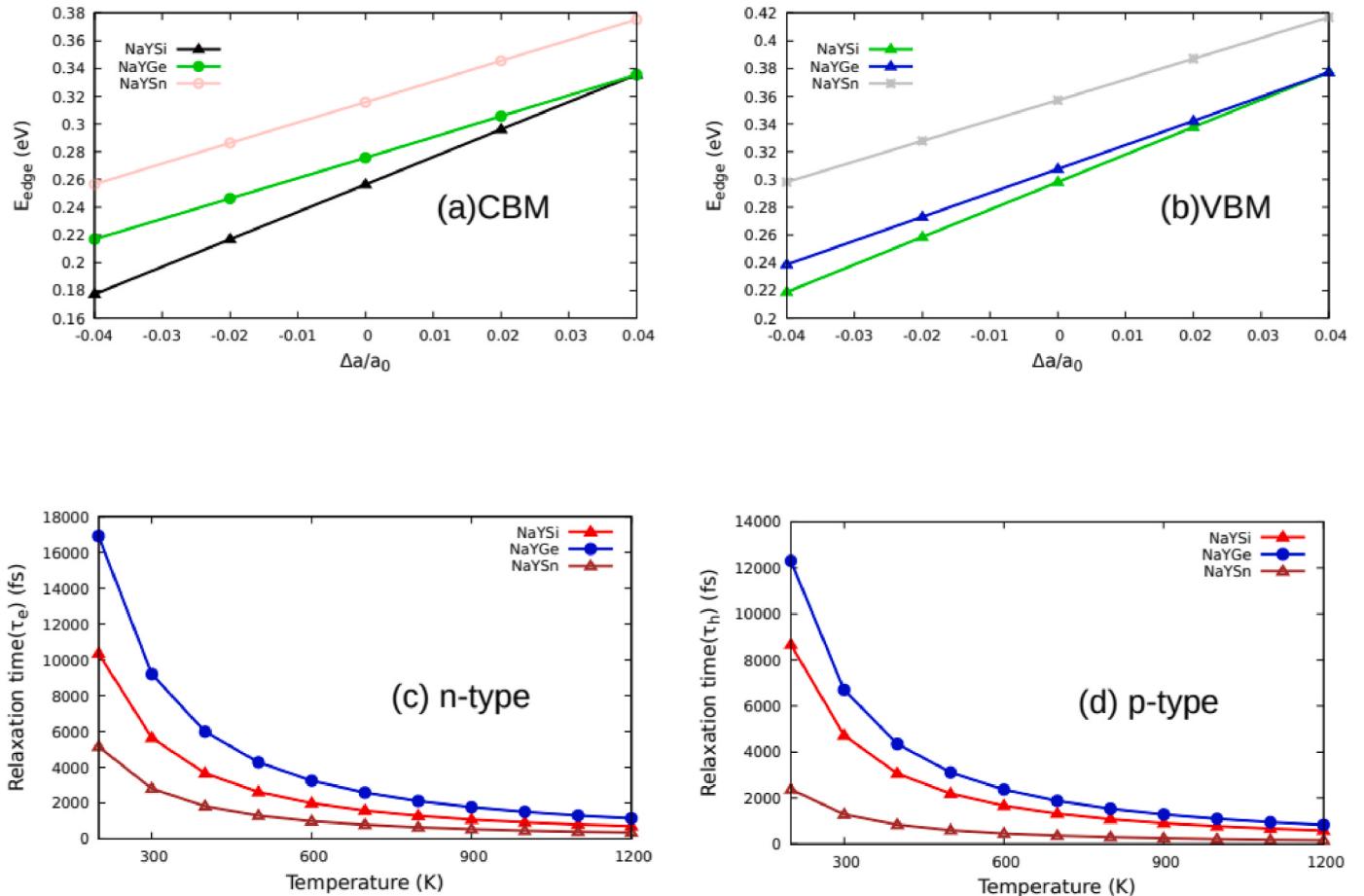


Fig. 7. (a) Variation of conduction band minimum (CBM) edges with fractional change in lattice constants, (b) Variation of valence band maximum (VBM) edges with fractional change in lattice constants, (c) Relaxation time (τ_e) response to temperature for n-type charge carrier, (d) Relaxation time (τ_h) response to temperature for p-type charge carrier of NaYZ (Z = Si, Ge, Sn) compounds.

$$S = \frac{8\pi^2 K_B^2}{3eh^2} m^* T \left(\frac{\pi}{3n} \right)^{\frac{2}{3}} \quad (11)$$

The compounds band structures can be used to determine the variation and rough values of their Seebeck coefficients (S). The value of S is intimately related to the effective masses of the holes and electrons in the valence and conduction bands, as demonstrated by this Mott's formula. The CBM and VBM curvatures are used to roughly calculate the effective masses of the electron and hole, as was mentioned previously in the computing session. With regards to the findings shown in Table 2, NaYSi and NaYGe both have effective electron masses (m_e) of 0.270 and 0.269, respectively. This explains why both compounds approximations of the Seebeck coefficients in the n-type charge carrier are valid. Materials thermoelectric performance would be improved by higher Seebeck coefficients for p-type charge carriers as opposed to n-type carriers.

6.2. Electronic relaxation time (τ)

Using the deformation potential theory and effective masses of the charge carriers as indicated in Equation (1), the temperature dependent relaxation time of charge carriers ($\tau = F(T)$) is computed. The calculated deformation potentials (E_a) and the charge carriers relaxation time (τ_e , τ_h) for NaYZ (Z = Si, Ge, Sn) are illustrated in Fig. 7. In Fig. 7(a) and (b), E_a is explained as the variation of band edges in conduction band and valence band to its fractional lattice constants as expressed in equation (2). The electrical conductivity, electronic thermal conductivity and power factor are derived as explicit dimensions (units) of S/m, W m⁻¹, W m⁻¹ K⁻² respectively, using the results obtained as $\tau = F(T)$. The

deformation potentials and temperature dependent relaxation time ($\tau = F(T)$) for the compounds at room temperature are stated in Table 2. These results are comparable to the deformation potentials and relaxation time charge carriers recently computed for half-Heusler alloys as reported in Refs. [49,50]. Also, it is worthy of note that the deformation potential between the conduction band and valence band for each of the compound is relatively the same except for NaYGe compound. Its covalent bond nature confirmed by Poisson ratio is suspected to be the reason for this deviation among others with ionic bonds. Fig. 10 illustrated that the electron relaxation time (τ_e) and hole relaxation (τ_h) time decreases as the temperature rises; this pattern shows that both τ_e and τ_h are more sensitive at lower temperatures (100 K–400 K) and become constants at higher temperatures. The relaxation time of hole charge carrier (τ_h) is smaller compared to electron (τ_e), this is due to difference in the effective masses of hole and electron. In the same way, NaYSn compound has the least relaxation time for both p and n-type carriers compared to NaYSi and NaYGe compounds due to its relatively large effective masses of hole and electron. This observation is obvious for the reason that relaxation time charge carrier (τ) is inversely related to the effective mass of charge carrier (m_h , m_e) validated by the expression in Equation (1).

6.3. Electrical conductivity (σ) and power factor ($S^2\sigma$)

The p-type thermoelectric properties of NaYZ (Z = Si, Ge, Sn) including electrical conductivity, total thermal conductivity, power factor and figure of merit, are shown in Fig. 8. Fig. 8(a) illustrates the p-type charge carrier of electrical conductivity (σ) of the NaYZ (Z = Si, Ge,

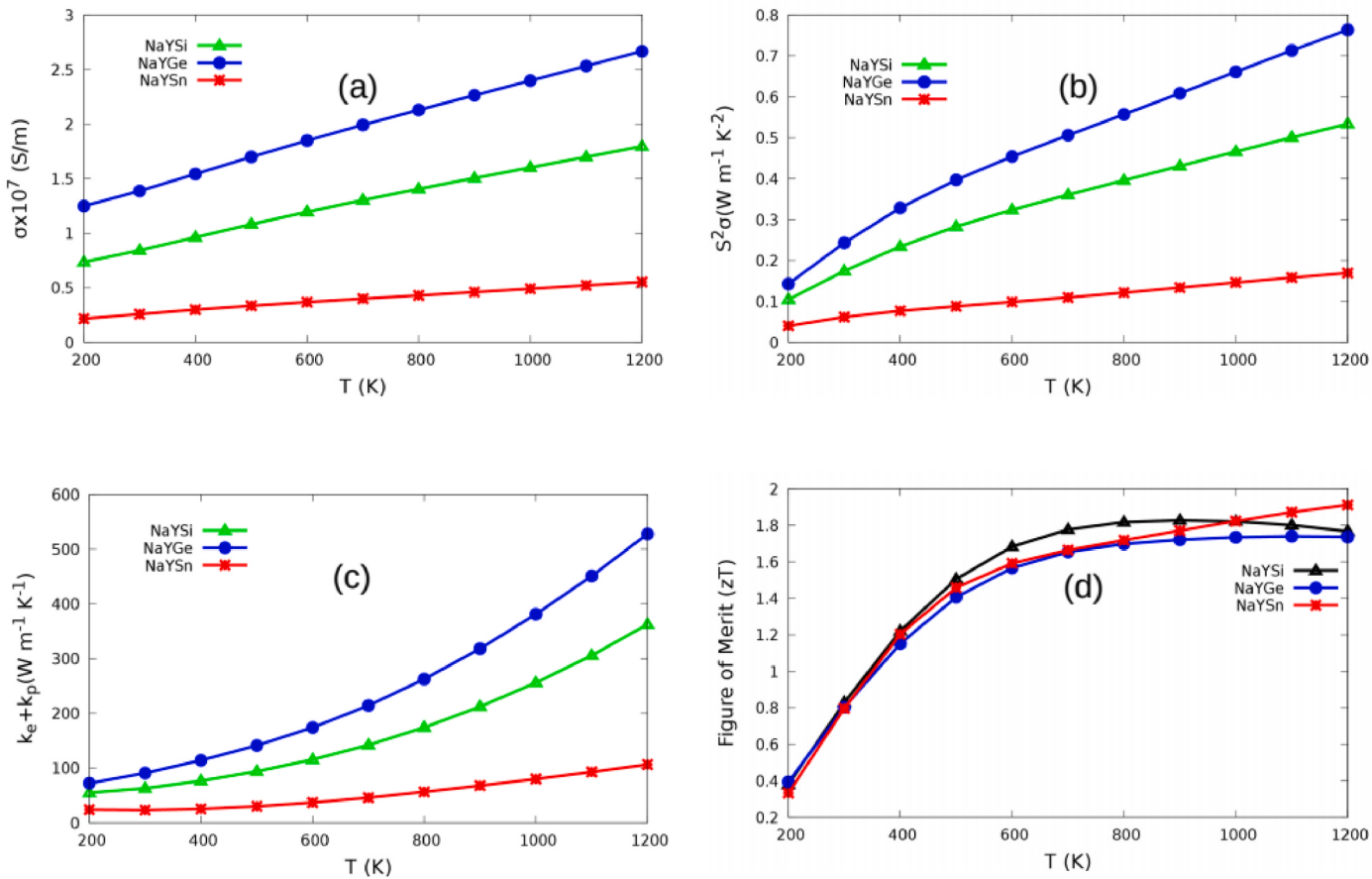


Fig. 8. (a) Electrical conductivity (σ), (b) Power factor ($S^2\sigma$), (c) Total thermal conductivity ($k_e + k_p$), (d) Figure of merit (zT) against temperature (p-type) of NaYZ ($Z = \text{Si, Ge, and Sn}$) half-Heusler compounds.

and Sn) against temperature (200 K–1200 K). The σ s of NaYGe and NaYSi compounds both rise significantly with temperature, whereas the σ of NaYSn compound only slightly rises with temperature due to its heavy effective mass of hole and electron, this is also explained by the low speed (low mobility) of the charge carrier ($\sigma \propto \frac{1}{m^*}$ and $\mu = \frac{e\tau}{m^*}$). The n-type carrier of σ against temperature is depicted in Fig. 9 (a) for all the compounds NaYZ ($Z = \text{Si, Ge, Sn}$). At high temperature, NaYGe compound has the highest value of σ , followed by NaYSi and NaYSn compound respectively; a pattern similar to the p-type curve of σ . Due to its inverse relationship with the effective mass of charge carrier(s) as previously stated, the compound with a high effective mass of electron (hole) tends to have the least or lowest value of σ and carrier mobility ($\sigma = ne\mu$). In contrast to the p-type σ curve against temperature, the n-type curve of σ is slightly nonlinear.

Figs. 8(b) and 9(b), respectively, show temperature dependence of the p-type and n-type charge carriers of the power factor ($S^2\sigma$) for NaYZ ($Z = \text{Si, Ge, Sn}$). In contrast to the n-type curve, the p-type power factor curve is linear. Compared to the p-type, the n-type charge carrier has a large power factor. At 1200 K, NaYSi has a p-type power factor of 0.52 W m⁻¹ K⁻², NaYGe of 0.77 W m⁻¹ K⁻², NaYSn of 0.18 W m⁻¹ K⁻² while NaYSi has an n-type power factor of 0.60 W m⁻¹ K⁻², NaYGe of 0.97 W m⁻¹ K⁻² and NaYSn of 0.26 W m⁻¹ K⁻². The NaYGe compound has the highest power factor for both p-type and n-type carriers among these half-Heusler compounds. Also, NaYGe has a distinctive pattern of conduction bands at the Γ point, which may be attributed to its high power factor on both p-type and n-type carriers in addition to its high relaxation time and least effective masses of charge carriers.

6.4. Total thermal conductivity ($k_e + k_p$)

Figs. 8 (c) and Fig. 9 (c), respectively, display the overall thermal conductivity of the p-type and n-type carriers of NaYZ compounds. The contributions of the electronic (k_e) and phonon (k_p) are combined to form total thermal conductivity, or $k_e + k_p$. Equations (3) and (4) are used to compute k_p using the modified Slack's model. This Slack's model is distinct because the results were adjusted to fall within the experimental range of k_p by obtaining an optimized A constant that captured all the features of A_{exp} (experimental constant), aligning the result with referenced experimental standards. Fig. 10 displays the computed k_p based on the modified Slack's model for NaYZ ($Z = \text{Si, Ge, Sn}$). At room temperature, the values of k_p are 17.265, 14.671, and 10.693 for NaYZ ($Z = \text{Si, Ge, Sn}$) respectively. These values are within the range of k_p values that have been reported in earlier studies [51,52]. Figs. 8(a) and 9 (c) respectively, show the sum of k_p and k_e for p-type and n-type carriers changes with temperature. As temperature rises, the sum of k_e and k_p on the p-type carrier reveals a nonlinear pattern with an upward trend as illustrated in Fig. 8 (a). Fig. 9 (c) depicts the n-type curve of total thermal conductivity as a function of temperature is significantly higher than the p-type according to our overall observation. The Wiedemann-Franz law stated as $k_e = \sigma LT$ [53] explains temperature dependent of k_e pattern as predicted by our results. While the computed lattice thermal conductivity k_p first exhibits a sharp decrease with temperature rise, but become constant (temperature independent) at higher temperatures due to growth in anharmonicity of the compounds [54].

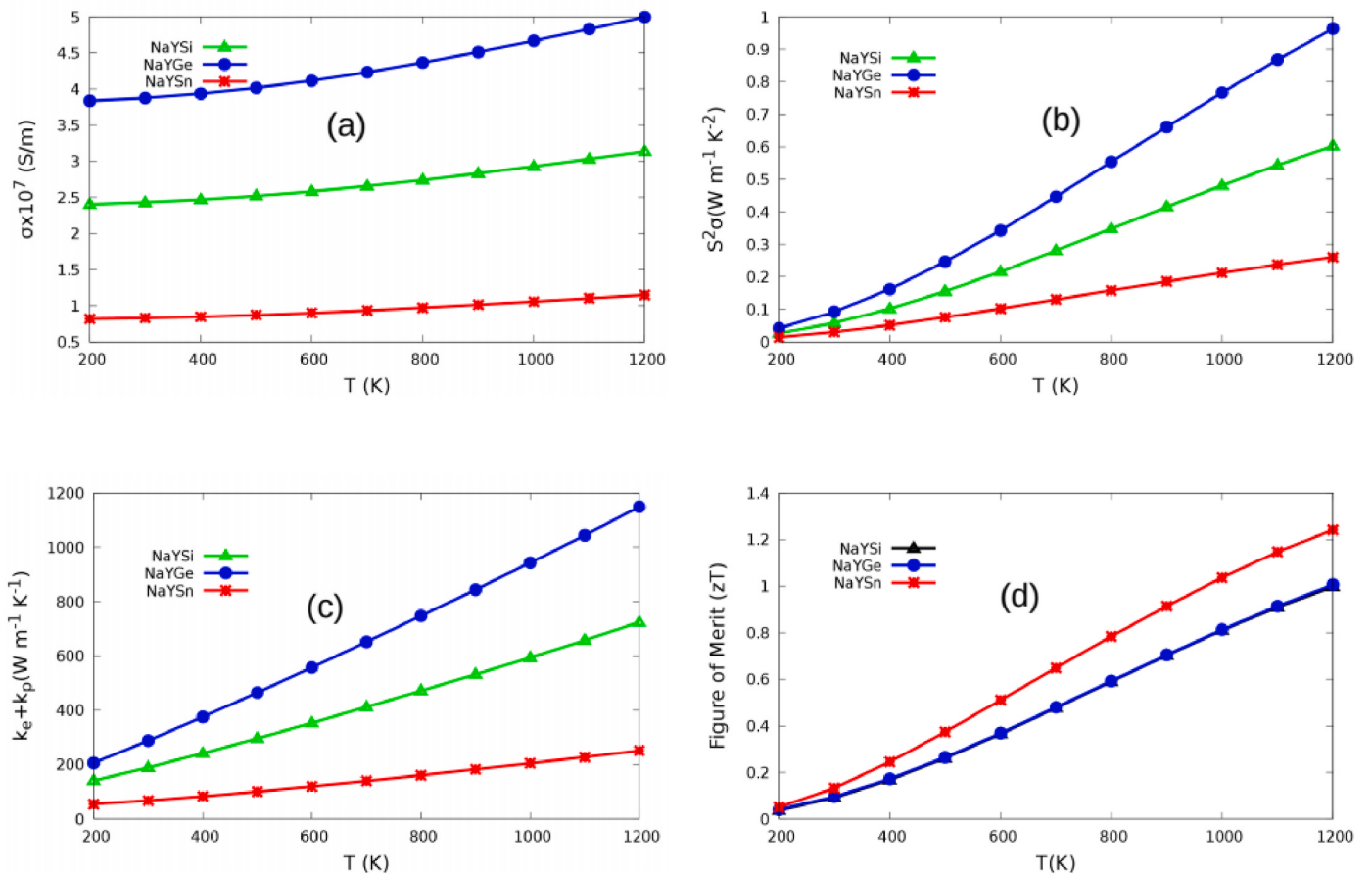


Fig. 9. (a) Electrical conductivity (σ), (b) Power factor ($S^2 \sigma$), (c) Total thermal conductivity ($k_e + k_p$), (d) Figure of merit (zT) Variation with temperature (n-type) of NaYZ (Z = Si, Ge, and Sn) compounds.

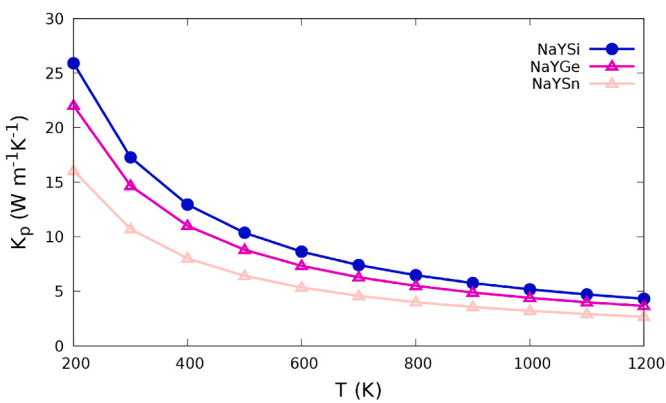


Fig. 10. The modified Slack's model results of lattice thermal conductivity (k_p) of NaYZ (Z = Si, Ge, and Sn) compounds.

6.5. Figure of merit

Figs. 8 (d) and 9 (d) respectively, show the figure of merit (zT) of the half-Heusler compounds NaYZ (Z = Si, Ge, and Sn) for p-type and n-type plotted against temperature. For all the compounds, the p-type zT curve considerably increases nonlinearly with temperature. It is clear that all compounds zT reached a value of 0.8 at room temperature. The NaYSi compound's zT curve climbs up to 900 K and achieves a zT value of 1.82 before starting to fall. The zT value of NaYGe reaches 1.73 at 1000 K and remains stable up to 1200 K. The NaYSn compound's zT curve rises steadily with temperature and reaches a maximum value of 1.91 at 1200

K. These calculated zT are comparable to or higher than the zT of the well-known thermoelectric materials such as p-type of NbFeSb ($zT = 1.0$), p-type TaFeSb ($zT = 1.5$) at 1000 K and others [55–59]. The n-type zT curve is linear with respect to temperature, reaching a maximum zT value of 1.22 for the NaYSn compound at 1200 K. At room temperature, all of the compounds (n-type) zT values are less than 0.2. Due to a high Seebeck coefficient, a high power factor, and low thermal conductivity, the overall thermoelectric attributes performance is in the p-type region.

Furthermore, we analyze zT (figure of merit) against temperature for NaYZ (Z = Si, Ge, Sn) at constant relaxation time ($\tau = 10^{-13}$ s) and then compare the results with those obtained for relaxation time that is temperature-dependent ($\tau = F(T)$). Fig. 11 (b) exhibits the constant relaxation time ($\tau = 10^{-13}$ s) response on zT for both p- and n-type carriers in contrast to Fig. 11 (a), which depicts the temperature-dependent relaxation time effect on the figure of merit (zT). As the temperature increases, the same pattern is seen in the curves on the p-type and n-type carriers. All of the half-Heusler compounds achieved 0.8 values for the figure of merit at room temperature for $\tau = F(T)$ in the p-type carrier. While the constant relaxation time is $\tau = 10^{-13}$ s, zT values (p-type carrier) at room temperature are 0.36 for both NaYSi and NayGe compounds, 0.62 for the NaYSn compound. Also, the values of zT at higher temperatures (600 K, 900 K, and 1200 K) for $\tau = F(T)$ are (1.68, 1.82, 1.76) NaYSi, (1.56, 1.72, 1.73) NaYGe, (1.59, 1.77, 1.91) NaySn and with the use of $\tau = 10^{-13}$ s are (1.23, 1.61, 1.67) NaySi, (1.19, 1.54, 1.65) NaYGe, (1.45, 1.72, 1.88) NaYSn compounds respectively. These figure of merit (zT) obtained with temperature dependent relaxation time ($\tau = F(T)$) are higher than the ones with constant relaxation time ($\tau = 10^{-13}$ s). This observation can be aligned with heavy bands structures of NaYZ (Z = Si, Ge, Sn) compounds and the effects of deformation

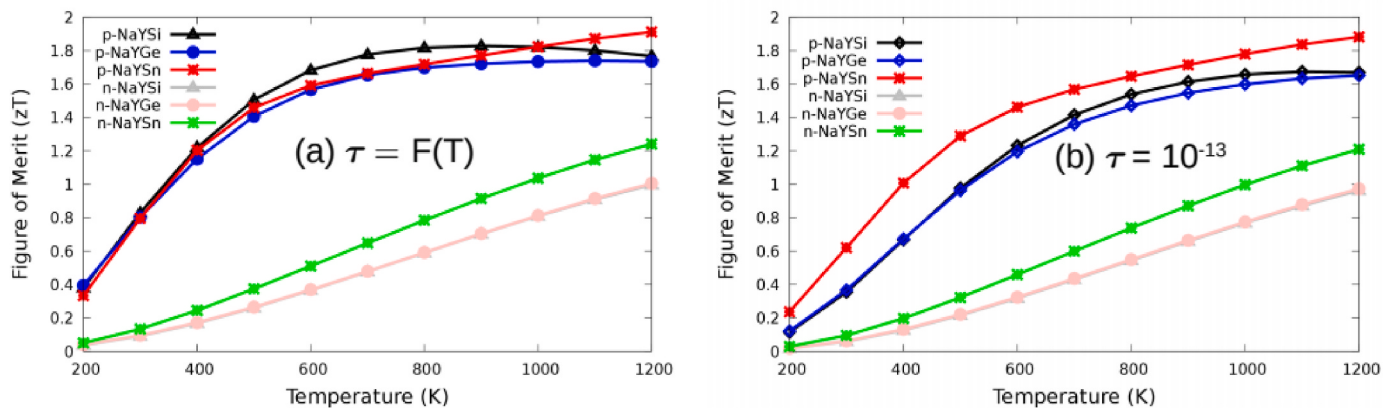


Fig. 11. Figure of merit response to (a) Temperature dependent relaxation time $\tau = F(T)$ and (b) Constant relaxation time ($\tau = 10^{-13}$ s) of NaYZ (Z = Si, Ge, and Sn) half-Heusler compounds.

potential theory which is never put into consideration with constant relaxation time approximation. The n-type carrier curves of zT against temperature in Fig. 11 (a) and (b) follows the same linear pattern with temperature rise for both temperature dependent relaxation ($\tau = F(T)$) and ($\tau = 10^{-13}$ s) for all the compounds. Although zT values at room temperature is small and insignificant in both cases for the n-type carriers. The maximum zT attains with $\tau = F(T)$ and $\tau = 10^{-13}$ s at 1200 K are (1.24, 1.20) NaYSn, (1.00, 0.97) NaYGe and (1.00, 0.96) NaYSi, respectively. These results revealed that NaYSn compound remains the overall best candidate with high thermoelectric performance among others in both cases ($\tau = F(T)$ and $\tau = 10^{-13}$ s) at room temperature and higher temperatures. NaYSi and NaYGe compounds curves exhibits slight differences in thermoelectric properties and this is confirmed by the overlapping of the two curves displayed in n-type regions both in temperature dependent relaxation time ($\tau = F(T)$) and $\tau = 10^{-13}$ s as shown in Fig. 11. These analysis show that both p and n-type of half-Heusler Na-based compounds have notable thermoelectric attributes at high temperatures and this research could also serve as a template for further experimental work to unveil more of its thermoelectric properties.

7. Conclusion

The electronic, structural, lattice dynamics, elastic as well as thermoelectric properties of the new half-Heusler alloys NaYZ (Z = Si, Ge, Sn) were predicted via density functional theory and semi-classical Boltzmann transport theory. Our reported structural optimization calculations have shown that ZXY phase with the least energy is the most stable structure. The calculated lattice constants obtained were observed to increase with the mass number of NaYZ (Z = Si, Ge, Sn). Also, the elastic constants computed were examined with the Born-Huang criteria for elastic and mechanical stability of the materials; these criteria were satisfied and the materials are elastically and mechanically stable. The electronic band calculations shown in the electronic band structure validated a direct band gap nature at point X along the high symmetry for all the compounds. The energy band gaps calculated for the new half-Heusler were 0.535, 0.571, 0.653 (in eV) for NaYSi, NaYGe, NaYSn compounds respectively. Dispersion phonon band structures for lattice dynamics computed with Density perturbation theory (DEPT) were found to be stable with the existence of positive frequencies all through the phonon band structures. Thermoelectric properties were examined with Boltzmann transport theory as implemented in BoltzTraP2 with deformation potential theory. The carriers' relaxation time for all the compounds were computed using the effective masses of the charge carriers along with deformation potentials to explicitly explain the thermoelectric performance. The results shown through zT curve against temperature in p-type and n-type regions revealed that p-type carrier

have better thermoelectric performance as compared with n-type. The figure merit (zT) for p-type (NaYZ, Z = Si, Ge, Sn) at room temperature is 0.8, while the n-type value is 0.09 (NaYSi), 0.09 (NaYGe), 0.14 (NaYSn). Furthermore, we compared the effect of constant relaxation time (τ) approximation with temperature dependent relaxation time $\tau = F(T)$ on zT of NaYZ (Z = Si, Ge, Sn). Our results revealed that the constant relaxation time approximation ($\tau = 10^{-13}$ s) effects on thermoelectric performance (zT) has minimal influence as compared with temperature dependent relaxation time $\tau = F(T)$. Finally, the p-type carrier of these half-Heusler alloys NaYZ (Z = Si, Ge, Sn) have high zT value of 0.8 at room temperature and at higher temperatures (900 K, 1000 K, 1200) 1.82, 1.73, and 1.91 respectively. These present results of figure of merits (zT) suggest that the materials under consideration are thermoelectric efficient both at room temperature and higher temperatures.(see Fig. 11)

CRediT authorship contribution statement

Olusola G. Adeleye: Conceptualization, Data Collection, Formal analysis. **Bamidele I. Adetunji:** Conceptualization, Supervision, Approval of version of manuscript to be published. **Abdulahi N. Njah:** Conceptualization, Supervision, Approval of version of manuscript to be published. **Olasunkanmi I. Olusola:** Conceptualization, Supervision, Approval of version of manuscript to be published.

Declaration of competing interest

The authors declare that they have no known competing financial interests or personal relationships that could have appeared to influence the work reported in this paper.

Data availability

Data will be made available on request.

Acknowledgement

OGA and BIA would like to acknowledge Dr Mulwa Winfred Mueni and the Center for High Performance Computing (CHPC) South Africa for the computational resources used to perform this research.

References

- [1] Joseph R. Sootsman, Duck Young Chung, Mercouri G. Kanatzidis, New and old concepts in thermoelectric materials, *Angew. Chem. Int. Ed.* 48 (46) (2009) 8616–8639.

- [2] Anubhav Jain, Yongwoo Shin, Kristin A. Persson, Computational predictions of energy materials using density functional theory, *Nat. Rev. Mater.* 1 (1) (2016) 1–13.
- [3] Yanzhong Pei, Heng Wang, G Jeffrey Snyder, Band engineering of thermoelectric materials, *Adv. Mater.* 24 (46) (2012) 6125–6135.
- [4] Bed Poudel, Hao Qing, Yi Ma, Yucheng Lan, Minnich Austin, Bo Yu, Xiao Yan, Dezhai Wang, Andrew Muto, Daryoosh Vashaee, et al., High-thermoelectric performance of nanostructured bismuth antimony telluride bulk alloys, *Science* 320 (5876) (2008) 634–638.
- [5] Jun Mao, Yumei Wang, Zihang Liu, Binghui Ge, Zifeng Ren, Phonon scattering by nanoscale twin boundaries, *Nano Energy* 32 (2017) 174–179.
- [6] Peeyush Kumar Kamlesh, Sarita Kumari, Ajay Singh Verma, et al., Effect of hybrid density functionals on half-heusler liznx ($x = n, p$ and as) semiconductors: potential materials for photovoltaic and thermoelectric applications, *Phys. Scripta* 95 (9) (2020), 095806.
- [7] F. Parvin, M.A. Hossain, I. Ahmed, K. Akter, A.K.M.A. Islam, First-principles calculations to investigate mechanical, optoelectronic and thermoelectric properties of half-heusler p-type semiconductor baagp, *Results Phys.* 23 (2021), 104068.
- [8] Takayuki Kojima, Satoshi Kameoka, An-Pang Tsai, The emergence of heusler alloy catalysts, *Sci. Technol. Adv. Mater.* 20 (1) (2019) 445–455.
- [9] Hsin Chao, C-K Yang Thomas, Sea-Fue Wang, Shi-Quan Lu, The sputtering of heusler alloy catalyst onto the porous anode of the intermediate temperature solid oxide fuel cells for ammonia disassociation, *ECS Trans.* 91 (1) (2019) 361.
- [10] Jiong Yang, Huanning Li, Ting Wu, Wenqing Zhang, Lidong Chen, Jihui Yang, Evaluation of half-heusler compounds as thermoelectric materials based on the calculated electrical transport properties, *Adv. Funct. Mater.* 18 (19) (2008) 2880–2888.
- [11] G. Rogl, A. Grytsiv, M. Gürth, A. Tavassoli, C. Ebner, A. Wünschek, S. Puchegger, V. Sopranyuk, W. Schranz, E. Bauer, et al., Mechanical properties of half-heusler alloys, *Acta Mater.* 107 (2016) 178–195.
- [12] Di Xiao, Yugui Yao, Wanxiang Feng, Jun Wen, Wenguang Zhu, Xing-Qiu Chen, G. Malcolm Stocks, Zhenyu Zhang, Half-heusler compounds as a new class of three-dimensional topological insulators, *Phys. Rev. Lett.* 105 (9) (2010), 096404.
- [13] F. Casper, T. Graf, S. Chadov, B. Balke, C. Felser, Half-heusler compounds: novel materials for energy and spintronic applications, *Semicond. Sci. Technol.* 27 (6) (2012), 063001.
- [14] Alexander Page, P.F.P. Poudeu, Ctirad Uher, A first-principles approach to half-heusler thermoelectrics: accelerated prediction and understanding of material properties, *Journal of Materials* 2 (2) (2016) 104–113.
- [15] Roberta Farris, Maria Barbara Maccioni, Alessio Filippetti, Vincenzo Fiorentini, Theory of thermoelectricity in mg3sb2 with an energy-and temperature-dependent relaxation time, *J. Phys. Condens. Matter* 31 (6) (2018), 065702.
- [16] Giulio Casu, Andrea Bosin, Vincenzo Fiorentini, Efficient thermoelectricity in sr 2 nb 2 o 7 with energy-dependent relaxation times, *Phys. Rev. Mater.* 4 (7) (2020), 075404, 17.
- [17] A. Azououi, A. Harbi, M. Moutaabbid, M. Idiri, A. Eddiai, N. Benzakour, A. Hourmatallah, K. Bouslykhane, R. Masrour, A. Rezzouk, First-principle investigation of lirsx ($x = p$ and as) half-heusler semiconductor compounds, *Indian J. Phys.* 97 (6) (2023) 1727–1737.
- [18] D.A. Pshenai-Severin, Yu I. Ravich, Calculations of the charge-carrier mobility and the thermoelectric figure of merit for multiple-quantum-well structure, *J. Semiconduct.* 36 (2002) 908–915. Springer.
- [19] Y. Benazouzi, H. Rozale, MA Boukli Hacene, M. Khethir, A. Chahed, D. Lucache, Electronic and thermoelectric properties in li-based half-heusler compounds: a first principle study, *Annals of West University of Timisoara-Physics* 61 (1) (2019) 44–55.
- [20] Dhurba R. Jaishi, Sujit Bati, Nileema Sharma, Bishnu Karki, Bishnu P. Belbase, Madhav Prasad Ghimire, Rhodiumbased half-heusler alloys as thermoelectric materials, *Phys. Chem. Chem. Phys.* 24 (33) (2022) 19844–19852.
- [21] Mosayeb Naseri, D.M. Hoat, First principles investigation on elastic, optoelectronic and thermoelectric properties of kyx ($x = ge, sn$ and pb) half-heusler compounds, *J. Mol. Graph. Model.* 92 (2019) 249–255.
- [22] Peeyush Kumar Kamlesh, Ruchita Gautam, Sarita Kumari, Ajay Singh Verma, Investigation of inherent properties of xscz ($x = li, na, k; z = c, si, ge$) half-heusler compounds: appropriate for photovoltaic and thermoelectric applications, *Phys. B Condens. Matter* 615 (2021), 412536.
- [23] Youcef Cherchab, Rafael Gonzalez-Hernandez, Structural stability and thermoelectric properties of new discovered half-heusler klax ($x = c, si, ge,$ and sn) compounds, *Computational and Theoretical Chemistry* (2021), 113231, 1200.
- [24] Xianfeng Ye, Zhenzhen Feng, Yongsheng Zhang, Gaofeng Zhao, David J. Singh, Low thermal conductivity and high thermoelectric performance via cd underbonding in half-heusler pcdna, *Phys. Rev. B* 105 (10) (2022), 104309.
- [25] Paolo Giannozzi, Stefano Baroni, Nicola Bonini, Matteo Calandra, Roberto Car, Carlo Cavazzoni, Davide Ceresoli, Guido L. Chiarotti, Matteo Cococcioni, Ismaila Dabo, et al., Quantum espresso: a modular and open-source software project for quantum simulations of materials, *J. Phys. Condens. Matter* 21 (39) (2009), 395502.
- [26] Andrea Dal Corso, Pseudopotentials periodic table: from h to pu, *Comput. Mater. Sci.* 95 (2014) 337–350.
- [27] Stefano Baroni, Stefano De Gironcoli, Andrea Dal Corso, Paolo Giannozzi, Phonons and related crystal properties from density-functional perturbation theory, *Rev. Mod. Phys.* 73 (2) (2001) 515.
- [28] H.S. Patel, V.A. Dabhi, A.M. Vora, Elastic constants of beryllium oxide: a first-principles investigation, in: *AIP Conference Proceedings*, ume 2224, AIP Publishing LLC, 2020, 030006.
- [29] Andrea Dal Corso, Elastic constants of beryllium: a first-principles investigation, *J. Phys. Condens. Matter* 28 (7) (2016), 075401.
- [30] Georg KH. Madsen, Jesús Carrete, Matthieu J. Verstraete, Boltztrap2, a program for interpolating band structures and calculating semi-classical transport coefficients, *Comput. Phys. Commun.* 231 (2018) 140–145.
- [31] J. Bardeen, W.J.P.R. Shockley, Deformation potentials and mobilities in non-polar crystals, *Physical review* 80 (1) (1950) 72.
- [32] Jinyang Xi, Mengqiu Long, Ling Tang, Dong Wang, Zhigang Shuai, First-principles prediction of charge mobility in carbon and organic nanomaterials, *Nanoscale* 4 (15) (2012) 4348–4369.
- [33] Guangzhao Qin, An Huang, Yiniao Liu, Huimin Wang, Zhenzhen Qin, Xue Jiang, Jijun Zhao, Jianjun Hu, Ming Hu, High-throughput computational evaluation of lattice thermal conductivity using an optimized slack model, *Materials Advances* 3 (17) (2022) 6826–6830.
- [34] Tomoo Katsura, Yoshinori Tange, A simple derivation of the birch–murnaghan equations of state (eos) and comparison with eos derived from other definitions of finite strain, *Minerals* 9 (12) (2019) 745.
- [35] Chathurangi Kumarasinghe, Neophytos Neophytou, Band alignment and scattering considerations for enhancing the thermoelectric power factor of complex materials: the case of co-based half-heusler alloys, *Phys. Rev. B* 99 (19) (2019), 195202.
- [36] Chenguang Fu, Haijun Wu, Yintu Liu, Jiaqing He, Xinbing Zhao, Tiejun Zhu, Enhancing the figure of merit of heavy-band thermoelectric materials through hierarchical phonon scattering, *Adv. Sci.* 3 (8) (2016), 1600035.
- [37] Chhatrasal Gayner, Yaron Amouyal, Energy filtering of charge carriers: current trends, challenges, and prospects for thermoelectric materials, *Adv. Funct. Mater.* 30 (18) (2020), 1901789.
- [38] Yunzhi Gao, Xiaofeng Liu, Wei Hu, Jinlong Yang, Tunable n-type and p-type doping of two-dimensional layered pdse₂ via organic molecular adsorption, *Phys. Chem. Chem. Phys.* 22 (23) (2020) 12973–12979.
- [39] Fanjie Kong, Yanfei Hu, Haijun Hou, Yanhua Liu, Baolin Wang, Lili Wang, Thermoelectric and thermodynamic properties of half-heusler alloy ypdsb from first principles calculations, *J. Solid State Chem.* 196 (2012) 511–517.
- [40] Akihiro Hori, Susumu Minami, Mineo Saito, Fumiuki Ishii, First-principles calculation of lattice thermal conductivity and thermoelectric figure of merit in ferromagnetic half-heusler alloy comnsb, *Appl. Phys. Lett.* 116 (24) (2020).
- [41] Nagendra S. Chauhan, Yuzuru Miyazaki, Low lattice thermal conductivity and microstructural evolution in vfesb half-heusler alloys, *Materialia* 22 (2022), 101430.
- [42] Q.Y. Xue, H.J. Liu, D.D. Fan, L. Cheng, B.Y. Zhao, J. Shi, Laptbsb: a half-heusler compound with high thermoelectric performance, *Phys. Chem. Chem. Phys.* 18 (27) (2016) 17912–17916.
- [43] Michael J. Mehl, Barry M. Klein, Dimitri A. Papaconstantopoulos, Intermetallic compounds: principle and practice, *Principles* 1 (1995) 195–210.
- [44] Hongzhi Fu, XiaoFeng Li, WenFang Liu, Yanming Ma, Tao Gao, Xinhua Hong, Electronic and dynamical properties of nial studied from first principles, *Intermetallics* 19 (12) (2011) 1959–1967.
- [45] Lei Qi, Yuchun Jin, Yuhong Zhao, Xiaomin Yang, Hui Zhao, Peide Han, The structural, elastic, electronic properties and debye temperature of ni3mo under pressure from first-principles, *J. Alloys Compd.* 621 (2015) 383–388.
- [46] Shuo Huang, Rui-Zi Li, San-Tao Qi, Bao Chen, Shen Jiang, A theoretical study of the elastic and thermal properties of scru compound under pressure, *Phys. Scripta* 89 (6) (2014), 065702, 18.
- [47] Diyou Jiang, Wenbo Xiao, Desheng Liu, Sanqiu Liu, Structural stability, electronic structures, mechanical properties and debye temperature of w-re alloys: a first-principles study, *Fusion Eng. Des.* 162 (2021), 112081.
- [48] Ken Kurosaki, Hironori Uneda, Hiroaki Muta, Shinsuke Yamanaka, Thermoelectric properties of thallium antimony telluride, *J. Alloys Compd.* 376 (1–2) (2004) 43–48.
- [49] Muktiyar Singh, et al., Augmented thermoelectric performance of licax ($x = as, sb$) half heusler compounds via carrier concentration optimization, *J. Phys. Chem. Solid.* 174 (2023), 111182.
- [50] Xilin Xiong, Rundong Wan, Zhengfu Zhang, Ying Lei, Guocai Tian, First-principle investigation on the thermoelectric properties of xcoge ($x = v, nb$, and ta) half-heusler compounds, *Mater. Sci. Semicond. Process.* 140 (2022), 106387.
- [51] Rajnish Kurchania, Utkarsh Namdeo, Yashi Jain, Deepika Srivastava, Analysing the structural, mechanical and thermal stability in lithium-based half-heusler compounds lialis and liajle: a first-principles study, *Bull. Mater. Sci.* 46 (3) (2023) 117.
- [52] Daniel Rabin, David Fuks, Yaniv Gelbstein, Alloying effect on the lattice thermal conductivity of mn3n half-heusler alloys, *Phys. Chem. Chem. Phys.* 25 (1) (2023) 520–528.
- [53] Salameh Ahmad, S.D. Mahanti, Energy and temperature dependence of relaxation time and wiedemann-franz law on phte, *Phys. Rev. B* 81 (16) (2010), 165203.
- [54] J.E. Turney, E.S. Landry, A.J.H. McGaughey, C.H. Amon, Predicting phonon properties and thermal conductivity from anharmonic lattice dynamics calculations and molecular dynamics simulations, *Phys. Rev. B* 79 (6) (2009), 064301.
- [55] Genadi Antonov Naydenov, Philip James Hasnip, V.K. Lazarov, M.I.J. Probert, Huge power factor in p-type half-heusler alloys nbfsb and tafsb, *J. Phys.: Materials* 2 (3) (2019), 035002.
- [56] Junhong Wei, Yongliang Guo, Guangtao Wang, Exploring structural, mechanical, and thermoelectric properties of half-heusler compounds rhbx ($x = ti, zr, hf$): a first-principles investigation, *RSC Adv.* 13 (17) (2023) 11513–11524.

- [57] Ioanna A. Ioannou, P-Type Half-Heusler and Bismuth-Telluride Thermoelectric Materials, 2022.
- [58] Kai Yang, Rundong Wan, Zhengfu Zhang, Ying Lei, Guocai Tian, First-principle investigation on the thermoelectric and electronic properties of hfco_x ($x = \text{as}, \text{sb}, \text{bi}$) half-heusler compounds, *J. Solid State Chem.* 314 (2022), 123386.
- [59] Z.F. Meghoufel, F. Cherifi, A. Boukra, F. Terki, Ab-initio investigation on the electronic and thermoelectric properties of new half-heusler compounds kbix ($x = \text{ba}$ and sr), *J. Phys. Condens. Matter* 33 (39) (2021), 395701.